Applied Catalysis B: Environmental 138–139 (2013) 1–8

Contents lists available at SciVerse ScienceDirect

Applied Catalysis B: Environmental

journal homepage: www.elsevier.com/locate/apcatb

Uniform hamburger-like mesoporous carbon-incorporated ZnO nanoarchitectures: One-pot solvothermal synthesis, high adsorption and visible-light photocatalytic decolorization of dyes

Mojiao Zhou [a], Xuehui Gao [a], Yong Hu [a,*], Jiafu Chen [b], Xiao Hu [c]

[a] Key Laboratory of the Ministry of Education for Advanced Catalysis Materials, Institute of Physical Chemistry, Zhejiang Normal University, Jinhua, 321004, PR China
[b] Hefei National Laboratory for Physical Sciences at Microscale, University of Science and Technology of China, Hefei, 230026, PR China
[c] School of Materials Science & Engineering, Nanyang Technological University, Singapore, 639798, Singapore

ARTICLE INFO

Article history:
Received 22 November 2012
Received in revised form 26 January 2013
Accepted 3 February 2013
Available online 26 February 2013

Keywords:
Mesoporous
Carbon-incorporated ZnO
Solvothermal synthesis
Adsorption
Photodecolorization

ABSTRACT

Uniform hamburger-like mesoporous carbon-incorporated ZnO (MC-ZnO) nanoarchitectures were facilely prepared by a simple, economical and environmentally benign solvothermal method using ethylene glycol (EG) as solvent in the presence of glucose. The as-obtained samples possessed a high surface area of 104 $m^2 g^{-1}$ and narrow pore size distribution around 7.2 nm. The adsorption behavior of Congo red (CR) onto the products fitted well the Langmuir isotherm and the adsorption process followed the pseudo-second-order kinetic model. The maximum adsorption capacity of CR as 162 $mg g^{-1}$ was achieved by Langmuir equation, while only 18.8 $mg g^{-1}$ was found for by commercial ZnO nanoparticles. Furthermore, the as-prepared nanoarchitectures exhibited enhanced photocatalytic activity for the decolorization of photosensitized dyes (CR and rhodamine-B) under visible-light illumination. Therefore, the MC-ZnO nanoarchitectures developed in this work may be a promising potential material for wastewater treatment.

1. Introduction

In recent years, the development of nanotechnology has extended from the stage of individual nanocomponent to that of three-dimensional (3D) stacking nanoarchitectures assembled from low-dimensional building blocks [1]. Up to now, a wide variety of inorganic materials have been successfully prepared with hierarchical shapes via various strategies [2–4]. Due to low cost and potential advantage for large-scale production, solution-phase chemical route was one of the most promising methods [5]. However, narrow size distribution and high dispersibility were the prerequisites for assembling [6]. Therefore, exploring rational and simple synthetic methods for controlling construction of complex 3D nanoarchitectures of functional materials remains as a challenging but exciting topic in materials science.

Zinc Oxide (ZnO), as one kind of versatile semiconductor nanomaterials, has been extensively applied in electronics, photoelectronics, optical devices and ecology owing to its significant quantum confinement effect, strong UV absorption properties, unique UV laser emission and excellent photocatalytic performance [7–9]. ZnO is extremely inclined to aligned along the c-axis to become the one-dimensional six prism shapes via a hydrothermal method [10]. However, the smaller aggregation rate allows ZnO particles have enough time to rotate so that further reduces the surface energy from the kinetic point of view in higher viscosity non-aqueous medium. By this way, there is certainly a strong thermodynamic driving force for oriented attachment to become nanospheres [11].

Herein, 3D uniform hamburger-like mesoporous carbon-incorporated ZnO (MC-ZnO) nanoarchitectures are obtained by a simple, economical and environmentally benign solvothermal method in ethylene glycol (EG) solution in the presence of glucose. In particular, this synthesis does not involve any surfactants or toxic materials. In this case, glucose not only acts as precursor of carbon incorporation, but also plays a critical role of coordinating reagent in reducing the activity of nanobuilding blocks to prevent the crystal lattice from fusing directly among ZnO nanoparticles and promote the ordered self-assembly [12]. A plausible formation mechanism has been proposed based on systematic investigation of the assembly process. With carbon incorporation, specific surface area and surface functional groups increased, the increasing electrostatic interaction and ion exchange reaction will further enhance adsorption capability [13,14]. Meanwhile, the photoresponce of ZnO can also extends toward visible light [15], resulting

* Corresponding author. Tel.: +86 579 82282234; fax: +86 579 82282595.
E-mail address: yonghu@zjnu.edu.cn (Y. Hu).

0926-3373/$ – see front matter © 2013 Elsevier B.V. All rights reserved.
http://dx.doi.org/10.1016/j.apcatb.2013.02.029

in the enhanced decolorization efficiency of dyes. Thus, the as-obtained 3D uniform hamburger-like MC-ZnO nanoarchitectures exhibit very promising performance in water treatment. As an example, we show that the products exhibit enhanced adsorption capability when evaluated as the adsorbents for the removal of dye pollutant Congo red (CR) from aqueous solution. For comparison, the removal capacity of CR by commercial ZnO nanoparticles was also studied. Additionally, the equilibrium isotherm and kinetic characteristics of CR adsorption on 3D uniform hamburger-like MC-ZnO nanoarchitectures were investigated thoroughly. On the other hand, the decolorization behaviors of CR and rhodamine-B (RhB) under visible-light irradiation were also investigated by using MC-ZnO nanoarchitectures, the as-obtained ZnO nanoparticles without glucose and commercial ZnO, respectively.

2. Materials and methods

All reagents were analytical grade, purchased from the Shanghai Chemical Reagent Factory, and used as received without further purification.

2.1. Synthesis of uniform hamburger-like MC-ZnO nanoarchitectures

In a typical procedure, 22 mL of 0.1 M zinc acetate ($Zn(Ac)_2{\cdot}2H_2O$) stock solution in EG was added with 10 mL of 0.6 M NaOH solution in EG, forming a milky mixture with pH value of 10.1. After stirring for about 10 min, 0.2 g of glucose was added and the resulting mixture was transferred into a 40 mL of Teflon-lined stainless steel autoclave, followed by heating at 160 °C for 24 h. Finally, the product was collected and washed with deionized water and ethanol for several times by centrifugation, then dried in an oven at 60 °C for 6 h, which was assigned code as sample A. To investigate the effect of carbon incorporated into ZnO nanoarchitectures, the sample was obtained by the similar procedure described as above except glucose was not added, which was named as sample B.

2.2. Characterization

Powder X-ray diffraction (XRD) measurements of the samples were performed with a Philips PW3040/60 X-ray diffractometer using Cu-Kα radiation at a scanning rate of $0.06^\circ\,s^{-1}$. Scanning electron microscopy (SEM) was performed with a Hitachi S-4800 scanning electron microanalyzer with an accelerating voltage of 15 kV. Transmission electron microscopy (TEM) and high-resolution transmission electron microscopy (HRTEM) were conducted at 200 kV with a JEM-2100F field emission TEM. Further evidence for the composition of the products was inferred from X-ray photoelectron spectroscopy (XPS), using an ESCALab MKII X-ray photoelectron spectrometer with Mg Kα X-ray as the excitation source. N_2 adsorption–desorption isotherms were obtained using a Micrometrics ASAP 2020. The absorption spectra were measured using a PerkinElmer Lambda 900 UV–vis spectrophotometer at room temperature. Thermogravimetric analysis (TGA) of the products was performed on a Netzsch STA 449 C thermal analyzer. N_2 adsorption–desorption isotherms were collected on a Micrometrics ASAP 2020 surface area and porosity analyzer at 77 K after the sample had been degassed in vacuum N_2 at 160 °C for 4 h.

2.3. Removal of CR

For the adsorption rate tests, 50 mg of hamburger-like MC-ZnO (sample A) and commercial ZnO nanoparticles adsorbents were added to 30 mL of CR ($100\,mg\,L^{-1}$) solutions under stirring, respectively, and stirring was continued for a certain time at room temperature. For adsorption isotherm studies, 30 mL of CR with different concentrations were mixed with 50 mg of sample A and commercial ZnO adsorbents for 2 h, respectively. After adsorption, solid and liquid were separated by centrifugation of the resulting suspension to measure the concentrations of CR in the solution. The measurements of CR concentrations were carried out using a UV–vis spectrophotometer, which was determined by measuring the solution absorbance at 496 nm.

2.4. Photodecolorization of CR and RhB

Photocatalytic activities of the as-prepared hamburger-like MC-ZnO were evaluated by the decolorization of CR and RhB under visible-light irradiation of a 500 W Xe lamp (CEL-HXF300) with a 420 nm cut off filter. The reaction cell was placed in a sealed black box with the top opened, and the cut off filter was placed to provide visible-light irradiation. All experiments were conducted at room temperature in air. In a typical process, 40 mg of as-prepared photocatalysts were added into 100 ml of CR solution (concentration: $50\,mg\,L^{-1}$) and RhB solution (concentration: $5\,mg\,L^{-1}$), respectively. After being dispersed in an ultrasonic bath for 5 min, the solution was stirred for 2 h in the dark to reach adsorption equilibrium between the catalyst and the solution and then was exposed to visible-light irradiation. The samples were collected by centrifugation at given time intervals to measure the dyes degradation concentration by UV–vis spectroscopy.

3. Results and discussion

XRD patterns reveal the phase and purity of as-obtained hamburger-like MC-ZnO nanoarchitectures assembled by ZnO nanoparticles, as shown in Fig. 1a All the reflection peaks can be indexed as the wurtzite phase of ZnO (JCPDS standard card no. 89-0511) with lattice constants of $a = 3.249$ Å and $c = 5.205$ Å. No additional peaks are detected, indicating the high purity of the sample. Based on the full width at half maximum of the diffraction peaks, the average size of ZnO nanoparticles is estimated as 5.8 nm by using the Debye–Scherrer equation. The small angle XRD pattern (inset in Fig. 1a) shows the peak at a low 2θ angle about 1.47°, which indicates that the as-prepared sample possesses a mesoporous structure. The mesoporous structures are less of long-range order because of the peak is broad and weak [16,17]. To give further insight into the porous structure and pore size distribution of the as-prepared samples, the Brunauer–Emmet–Teller (BET) method from the N_2 adsorption–desorption measurements and the pore size distributions from the adsorption and desorption branch of the N_2 isotherms by the Barrett–Joyner–Halenda (BJH) method were obtained. As shown in Fig. 1b, the N_2 adsorption–desorption isotherm of hamburger-like MC-ZnO nanoarchitectures exhibit type IV, indicating the existence of abundant mesoporous structures in the architectures [18]. A broad hysteresis loop in the relative pressure range from 0.5 to 1.0 is reported for materials comprised of aggregates (loose assemblages) of plate-like particles forming slit-like pores [19]. Moreover, a relatively narrow pore size distribution was seen from Fig. 1b (inset), showing a sharp peak at 7.2 nm. The as-obtained produces have a BET surface area of $104\,m^2\,g^{-1}$, which was almost 33 times higher than that of the commercial ZnO ($3.0\,m^2g^{-1}$) [20]. The high specific surface areas and narrow mesoporous channels were both favorable for improving adsorption capability.

The result of TGA of the as-obtained hamburger-like MC-ZnO nanoarchitectures further provide evidence that carbon incorporate into ZnO nanoarchitectures, as shown in Fig. 2. From the TGA curve (weight W vs temperature T plots), the ZnO content is about 79.6 wt%. A total weight loss of 20.4% was observed in the temperature range of 25–700 °C, in which the weight loss of 3.25% that

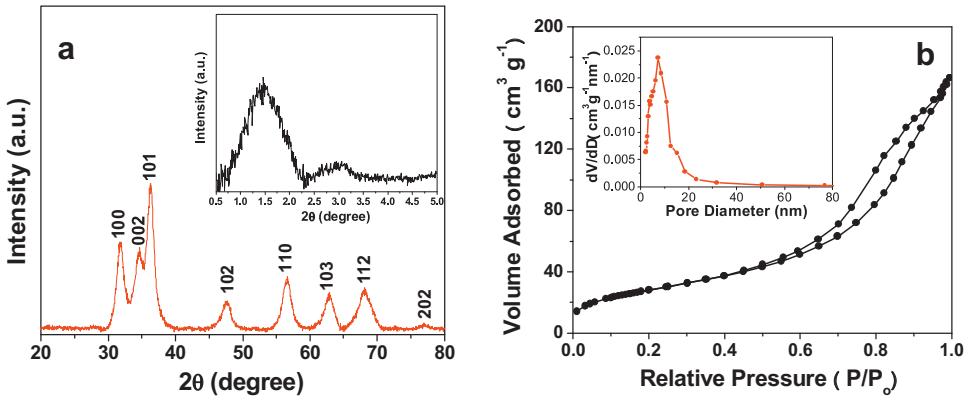

Fig. 1. (a) XRD pattern of the as-prepared hamburger-like MC-ZnO nanoarchitectures and small-angle XRD pattern (inset), (b) N_2 adsorption–desorption isotherm of the products, and corresponding pore size distribution (inset).

occurred at temperatures lower than 125 °C was caused by the evaporation of free water, and the weight loss of 14.5% in the range of 125–372 °C may be attributed to the desorption of bound water and the evaporation of EG. The final one at about 372–700 °C can be assigned to the removal of carbon residues, and about 2.66 wt% carbon can inferred in the products [21–24].

The states of the carbon incorporated into the hamburger-like MC-ZnO nanoarchitectures are further acquired with the XPS technique. The high-resolution spectrum of O 1s is shown in Fig. 3a, which can be de-convoluted into three peaks by the XPS peak fitting program. The peak at 530.2 can be attributed to the O^{2-} ions in the ZnO lattice, which is surrounded by Zn^{2+} ions [25]. And the peak at 531.5 eV should be assigned to surface oxygen species of O^{-} [26]. The higher binding energy peak at 532.5 eV may be attributed to different reasons, e.g. oxygen vacancies, hydroxyl group or the C—O bond [27]. Fig. 3b shows the C1s XPS spectrum of the as-prepared hamburger-like MC-ZnO nanoarchitectures. The core level spectrum in the C 1s region display an asymmetric broad peak, which indicated that more than one chemical state of C was present [28]. By fitting the experimental line profile, four peaks centered at 283.3, 284.6, 286.1, and 288.5 eV are identified, which can be assigned as the contributions from the Zn—C bonds (283.3 eV), the aromatic C—C bonds (284.6 eV), O—C—O complex (286.1 eV), and carbonate species (288.5 eV) [29]. The higher binding energy suggests the carbon may be incorporating into the interstitial positions of the ZnO lattice [30]. Thus, the XPS results suggest that the carbons can be indeed incorporated into the interstitial positions of ZnO lattice, and also the possibly of such defect complexes that involve C—O bonds.

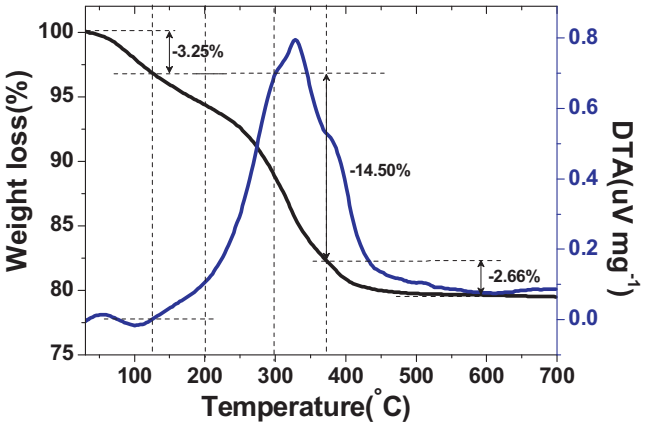

Fig. 2. Thermogravimetric analysis curve of the as-obtained hamburger-like MC-ZnO nanoarchitectures.

The morphology of the as-prepared 3D hamburger-like MC-ZnO nanoarchitectures is observed by SEM and TEM. A panoramic view of the as-obtained MC-ZnO nanoarchitectures reveals that the sample is entirely composed of uniform hierarchical hamburger-like nanohybrids with ~450 nm in diameter and ~600 nm in length, as shown in Fig. 4a. The high-magnification SEM image (Fig. 4b) and a single nanoarchitecture (Fig. 4c, indicated by white arrow in Fig. 4b) further display these hamburger-like nanoarchitectures are assembled from numerous primary particles as building blocks with size of several nanometers. The geometrical structure of as-prepared MC-ZnO nanoarchitectures is further elucidated by TEM results. From Fig. 4d and e, it is clearly seen that the hamburger-like nanostructure is composed of numerous single-crystal nanoplates and the disordered wormhole-like pores is observed in the midst of particles, indicating the formation of mesoporous structure. The pores are clearly intergranular pores templated by the organic species, which are different from those ordered pores created by polymer micelles. A representative HRTEM image is shown in Fig. 4f, from which the lattice spacing at 0.26 nm matches well with wurtzite phase of ZnO.

Time-dependent experiments are carried out to understand the formation process of such interesting 3D hamburger-like MC-ZnO nanoarchitectures. Fig. S1 shows SEM images of four samples obtained with different reaction durations, while keeping other conditions unchanged. Only particle subunits are formed at the early stage of the reaction (Figs. S1a, 3h). When the reaction time is increased from 6 to 12 h (Figs. S1b and c), the nanoparticles gradually congregate together and bread-like building blocks are formed. The well-defined hamburger-like nanoarchitectures only start to form after 18 h of solvothermal treatment (Fig. S1d). To investigate the effect of glucose and different solvent on the product morphology, a series of experiments are carried out. The SEM image of the samples obtained at 160 °C for 24 h in EG without presence of glucose is shown in Fig. S2 (Sample B). Fig. S3 shows SEM images of products prepared in distilled water (Fig. S3a) and ethanol (Fig. S3b), while keeping other conditions unchanged. Interestingly, it is found that all the products could not form hamburger-like morphologies. Thus, glucose and EG are two important roles in formation of hamburger-like MC-ZnO nanoarchitectures.

Based on the above experimental results, we speculate a possible formation mechanism for the development of uniform hamburger-like MC-ZnO nanoarchitectures, as illustrated in Scheme 1. It is well-known that ZnO has a basal positive polar plane (0 0 0 1) and a negative polar plane (0 0 0 $\bar{1}$), which is rich in

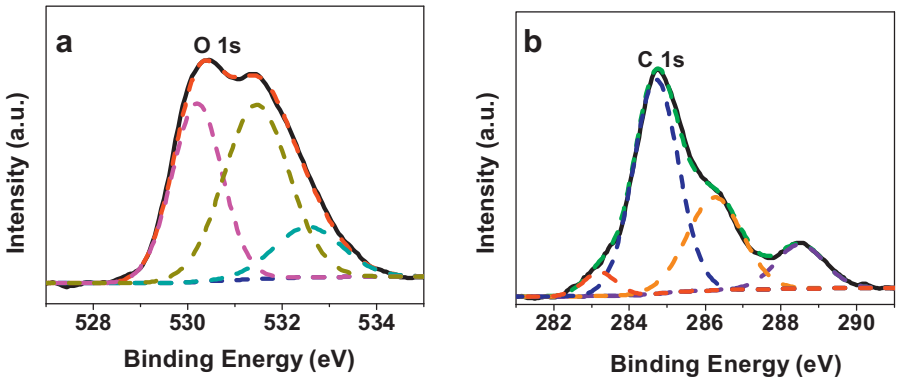

Fig. 3. XPS spectra of the as-prepared hamburger-like MC-ZnO nanoarchitectures: (a) O1s and (b) C1s binding energy spectra.

Zn^{2+} and O^{2-}, respectively [31]. Due to excellent chemical adsorption ability by means of complexes developing between anionic groups of EG and positive polar top surface of ZnO crystal, EG can affect the growth of ZnO crystal [32]. Similarly, growth orientation of ZnO is also affected by glucose, whose high negative charge will interact predominantly with the positively charged (0 0 0 1) faces of the ZnO crystals. These interactions reduce the surface free energy of positive planes and depress any directional growth of ZnO nuclei, resulting in equiaxed or spherical particle morphology. Under solvothermal conditions, various chemical reactions of glucose can take place, which lead to a complex mixture of some aromatic compounds and oligosaccharides [33,34]. These organic compounds can increase viscosity of the resulting solutions, in what has been denoted the "polymerization" step. The growth of the 3D

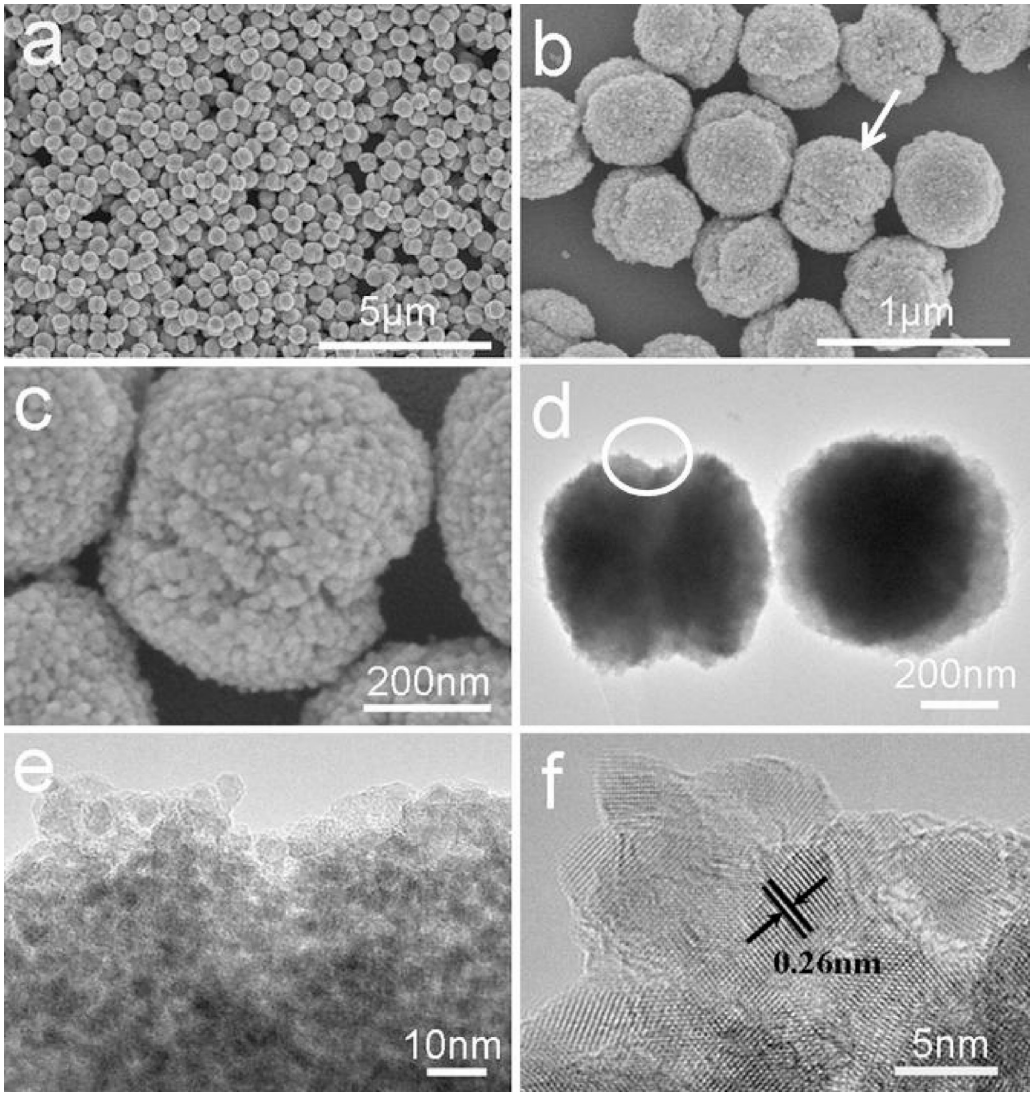

Fig. 4. SEM patterns of the as-prepared hamburger-like MC-ZnO (a, b and c). TEM (d and e) and HRTEM images (f) of the hamburger-like MC-ZnO.

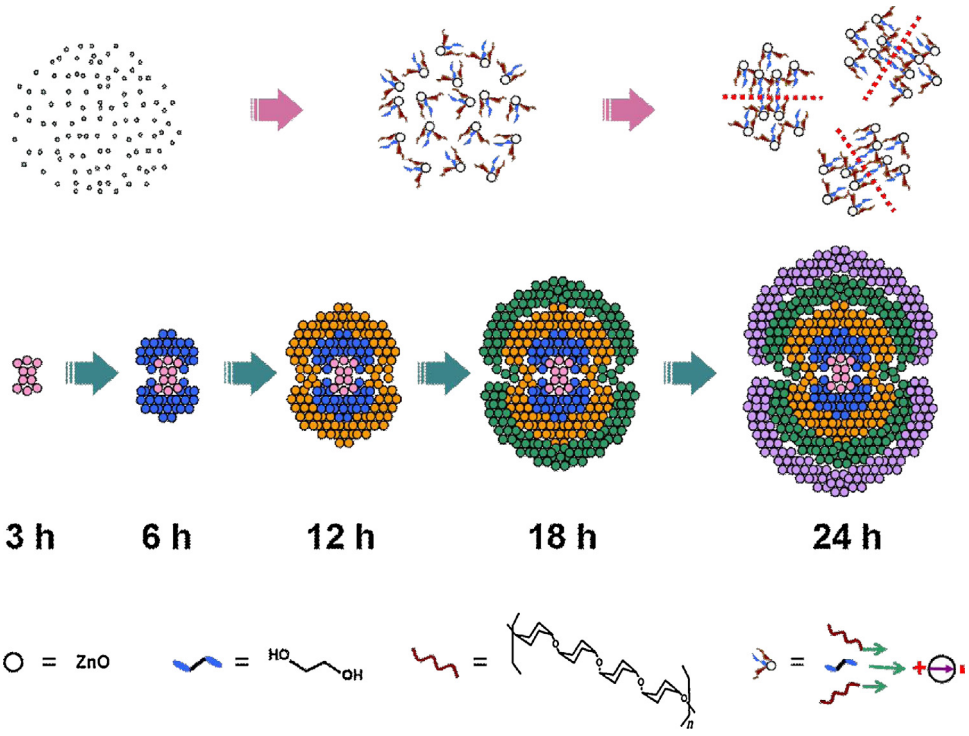

Scheme 1. Schematic illustration of the formation of 3D uniform hamburger-like MC-ZnO nanoarchitectures.

"twinning" superstructures occurs at this stages, which probably process via continuous adjoinment of additional oligosaccharides on the surface of ZnO subunits [35,36]. This twinning is allowed due to the adsorption of the polymers which counterbalance and possibly overcompensate the like charges on these faces, and self-assembly of these subunits may proceed via the stacking of their polar faces of opposite charge facing each other [37]. Furthermore, when the heating time is prolonged, carbonaceous polysaccharides are formed, which can adsorb Zn^{2+} to generate carbon-incorporated ZnO. In this case, glucose not only can confine the growth of ZnO nanocrystals, but also servers as an assembling agent to construct the nanoparticles into the 3D hamburger-like mesoporous superstructures.

Porous materials with high specific surface area are usually employed for waste water treatment due to their capability to adsorb a large quantity of pollutants [38,39]. With the incorporating of carbon, partially dehydrated residues in which reductive OH or CHO groups are covalently bonded to the carbon frameworks improve the hydrophilicity and stability of the products in aqueous systems [33]. In this case, we have investigated the application of the as-prepared hamburger-like MC-ZnO nanoarchitectures in water treatment. CR, a dye commonly used in the textile industry, is chosen as a model organic water pollutant [40]. Fig. 5a presents the effect of the contact time on the adsorption of CR by different absorbents with the initial CR concentration fixed at 100 mg L^{-1}. As can be seen, about 87% of CR is adsorbed within 1 min by hamburger-like MC-ZnO nanoarchitectures, and about 95% of CR is adsorbed after reached the equilibrium state in 60 min. As a comparison, only about 19% and 26% of CR is adsorbed within 1 min and 60 min by commercial ZnO nanoparticles. Adsorption isotherms can be described how the adsorbate interacts with adsorbent, which is the most important parameter for designing a desired adsorption system [41]. Fig. 5b shows the adsorption isotherms of CR on the different adsorbents at different initial concentrations of CR (50, 100, 150, 200, 250, 300, 350 and 400 mg L^{-1}). The as-prepared hamburger-like MC-ZnO nanoarchitectures obviously possesses a much higher removal capacity for CR than the commercial ZnO nanoparticles. For example, when the initial concentration of CR is 400 mg L^{-1}, the saturated adsorption capacity is 155 mg g^{-1}, while only 18.8 mg g^{-1} is found for by commercial ZnO. In order to investigate the reusability of the as-prepared hamburger-like MC-ZnO nanoarchitectures, cyclic adsorption–regeneration tests were carried out for CR (concentration: 100 mg L^{-1}). After adsorption process, the collected samples were added to 20 mL of 0.02 M NaOH solution under stirring for 1 h at room temperature. Then, the samples were washed with deionized water, and dried at 60 °C for 3 h. The regenerated samples were further used for adsorption–desorption of CR test. From Fig. 5c, it can be noticed that the adsorption capacity have no obvious decreases after five runs, which indicates that the as-prepared products can be regenerated and reused.

Adsorption kinetic experiments were further done to study the effect of contact time and evaluate properties. The amount of CR adsorbed at equilibrium was calculated from the following Eq. (1) [42]:

$$q_t = \frac{(C_0 - C_t)V}{m} \quad (1)$$

where q_t (mg g^{-1}) is the amount adsorbed per gram of adsorbent at time t (min), C_0 is the initial concentration of CR in the solution (mg L^{-1}), C_t is the concentration of CR at time t (mg L^{-1}), V is the volume of the solution (L), and m is the mass of the adsorbent used (g). To well understand the adsorption mechanism and kinetics, two well-known kinetic models, pseudo-first- and pseudo-second-order equations, are used to study the adsorption kinetics of the as-prepared hamburger-like MC-ZnO nanoarchitectures adsorbent [43,44]. The linear form of pseudo-first-order equation is given as follows [45]:

$$\ln(q_e - q_t) = \ln q_e - k_1 t \quad (2)$$

The values of q_e and k_1 can be calculated form the intercept and slope of $\ln(q_e - q_t)$ versus t, where k_1 is the rate constant of the pseudo-first-order model. Fig. 6a shows the correlation coefficient

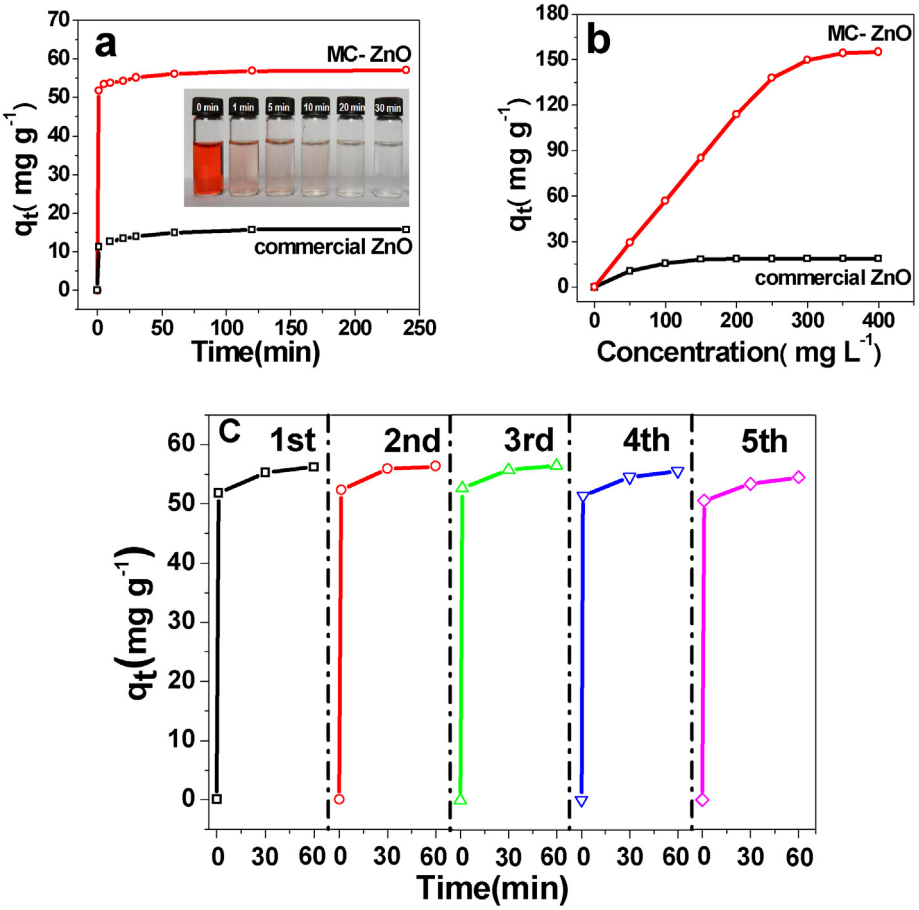

Fig. 5. (a) Effect of contact time on the adsorption of CR by hamburger-like MC-ZnO nanoarchitectures (inset: the change photographs of CR solution with the contact time) and commercial ZnO nanoparticles, the initial concentration of CR is 100 mg L^{-1}. (b) Adsorption isotherms for the adsorption of CR on MC-ZnO and commercial ZnO at room temperature. (c) Reusability of the as-prepared hamburger-like MC-ZnO nanoarchitectures for CR.

for CR is 0.7598, indicating the poor agreement of pseudo-first-order model with the experimental data.

The linear form of the pseudo-second-order equation is given as follows [46]:

$$\frac{t}{q_t} = \left(\frac{1}{k_2 q_e^2}\right) + \frac{t}{q_e} \quad (3)$$

As shown in Fig. 6b, linear plot of t/q_t against t exhibit high correlation coefficient of 0.9999. Thus, the adsorption is well consistent with the pseudo-second-order model.

Adsorption isotherms provide qualitative information on the capacity of the adsorbent as well as the nature of the solute surface interaction. In this study, Freundlich and Langmuir adsorption models were further employed to the analysis of our experimental data. The following Eq. (4) was used for Freundlich adsorption model [47].

$$\ln q_e = \ln K_F + b_F \ln C_e \quad (4)$$

where q_e (mg g^{-1}) is the amount of CR adsorbed at the equilibrium, C_e (mg L^{-1}) is the equilibrium concentration of CR in the solution, K_F is the Freundlich constant, and b_F is a constant depicting the adsorption capacity. Fig. 6c shows the value of ln q_e against ln C_e according to the experimental isotherm data. The low correlation coefficient (0.852) indicated the poor agreement with the Freundlich isotherm model.

The form of the Langmuir isotherm is as follows [48]:

$$\frac{C_e}{q_e} = \frac{C_e}{q_{max}} + \frac{1}{q_{max} K_L} \quad (5)$$

where q_{max} (mg g^{-1}) is the maximum capacity of the adsorbent, and K_L (L mg^{-1}) is the Langmuir adsorption constant. Fig. 6d presents the plot of C_e/q_e versus C_e and the correlation coefficients for CR is 0.999. Therefore, the adsorption of CR on the hamburger-like MC-ZnO nanoarchitectures fit with the Langmuir adsorption model better, implying that the adsorbed layer is monolayer coverage. From Langumir adsorption capacity of the products for CR was estimated to be 162 mg g^{-1}.

The photocatalystic activity of different samples was evaluated by decolorization of CR and RhB after exposure to visible light irradiation. Fig. 7a displays the photodecolorization behaviour of CR catalyzed by blank, commercial ZnO, the as-prepared ZnO nanostructures without glucose (Sample B) and hamburger-like MC-ZnO nanoarchitectures (Sample A), where C is the concentration of CR after different light irradiation times and C_0 is the initial concentration of the CR before dark adsorption. After visible light irradiation for 60 min, the decolorization fractions using commercial ZnO, sample B and sample A are about 22.3, 50.5 and 90.1%, respectively. This result indicates sample B is only slightly more active than commercial ZnO, but sample A exhibit enhanced photoactivity for CR decolorization. The enhanced decolorization efficiency of the as-prepared MC-ZnO nanoarchitectures may be ascribed to high specific surface area and carbon incorporation [49]. The carbon in MC-ZnO nanoarchitectures can be considered as an n-type surface modifier, which is understood that the interface contact and interaction between the two phases are rather intimated [50]. The UV–vis diffuse reflectance spectra of sample A and B (Fig. S4) further shows that the incorporating of carbon can improve the absorption of ZnO toward visible light (Fig. S4), indicating that more

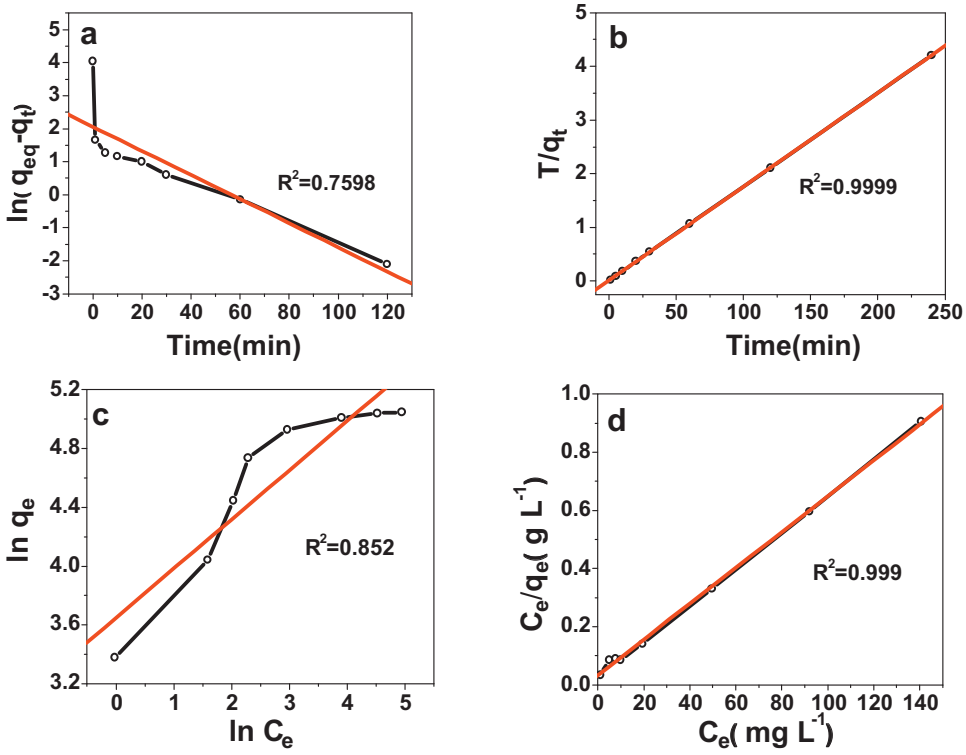

Fig. 6. Plots of (a) first- and (b) second-order rates for adsorption of CR onto MC-ZnO adsorbent. (c) The values of ln q_e against ln C_e based on the Freundlich isotherm model. (d) The linear dependence of C_e/q_e on C_e based on the Langmuir isotherm model.

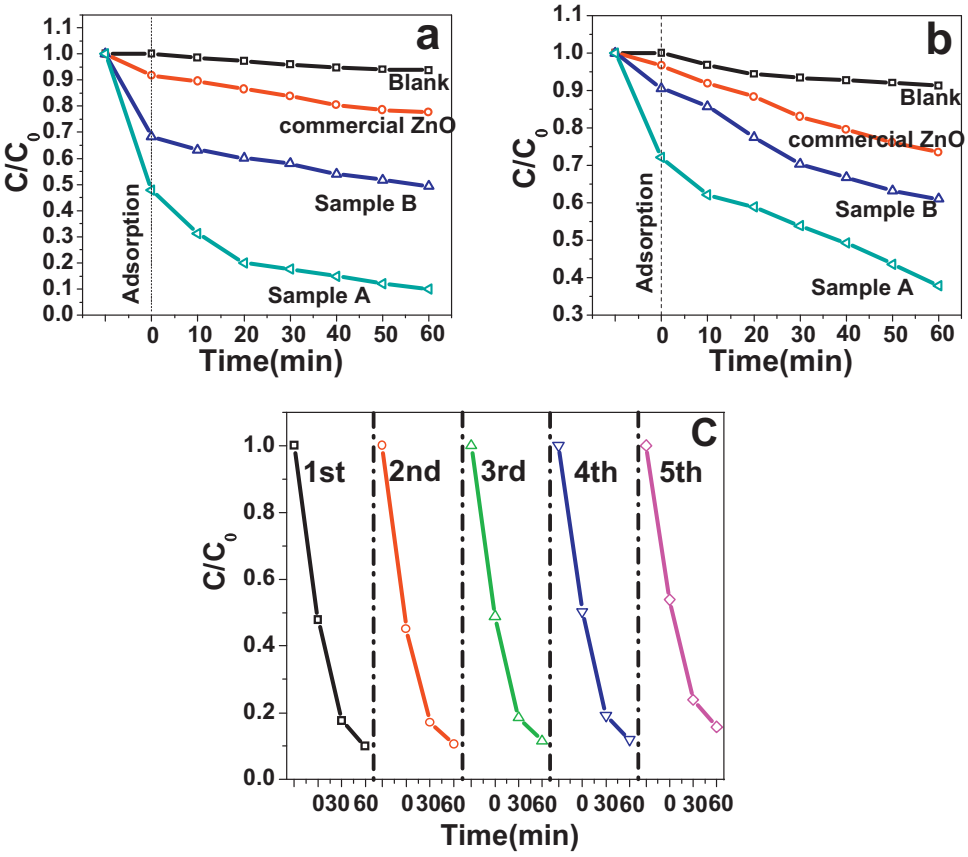

Fig. 7. Photocatalytic decolorization of (a) CR and (b) RhB in the blank test and using different samples: commercial ZnO nanoparticles, sample B and A. (c) 5 cycles of the decolorization of CR using sample A.

photons can be absorbed and be utilized for the photocatalytic reaction [21,51]. Additionally, MC-ZnO nanoarchitectures possess superior adsorption ability, and hence CR can be enriched on the surface of photoactive ZnO, resulting in the acceleration of the rate of photosensitization reaction [52,53]. Fig. 7b shows the photodecolorization behaviors of RhB, which exhibits a similar regularity like decolorization of CR. This result further demonstrates that hamburger-like MC-ZnO nanoarchitectures exhibit enhanced photoactivity for dyes decolorization under visible-light irradiation. We have further studied the stability and reusability of the photocatalyst used for the decolorization of CR by collecting and re-using the sample A for 5 cycles (Fig. 7c). The results show that there is only insignificant loss of the photocatalytic activity, which might be partly caused by the loss of the photocatalysts during each collection and rinsing step. From the SEM and TEM images (see Fig. S5 in the supporting information) and XRD pattern (Fig. S6) of sample A after 5 runs for the photodecolorization of CR, there are all no any obvious changes. Thus, it clearly demonstrates that the as-prepared products are quite stable and have great application potential in water treatment.

4. Conclusions

In this study, we developed a facile solvothermal route to synthesize uniform hamburger-like MC-ZnO nanoarchitectures in the presence of glucose, which concurred with "green" chemistry as it was simple and environmentally friendly. As carbon incorporated mesoporous self-assembly architectures, the samples have high surface area, superior adsorption capacity and enhanced photodecolorization of dyes under visible-light irradiation. The adsorption kinetics and isotherms studies demonstrated that the adsorption process obeyed the pseudo-second-order kinetics and Langmuir isotherm model, respectively. The maximum adsorption capacity was 162 mg g^{-1} calculated by Langmuir equation. It is believed that this facile strategy is scalable to synthesize other carbon-incorporated metal oxides and this fascinating adsorbent will find great potential applications in the adsorptions and decolorization of dyes from wastewaters.

Acknowledgments

Financial support from the Natural Science Foundation of China (21171146) and Zhejiang Provincial Natural Science Foundation of China (Y4110304) are gratefully acknowledged. J.F. Chen acknowledges the financial support from the Anhui Provincial Natural Science Foundation (11040606M53).

Appendix A. Supplementary data

Supplementary data associated with this article can be found, in the online version, at http://dx.doi.org/10.1016/j.apcatb.2013.02.029.

References

[1] H.Y. Xiao, Z.H. Ai, L.Z. Zhang, Journal of Physical Chemistry C 113 (2009) 16625–16630.
[2] Y.S. Ding, X.F. Shen, S. Gomez, H. Luo, M. Aindow, S.L. Suib, Advanced Functional Materials 16 (2006) 549–555.
[3] W.L. Yang, L. Zhang, Y. Hu, Y.J. Zhong, H.B. Wu, X.W. Lou, Angewandte Chemie International Edition 51 (2012) 11501–11504.
[4] Z. Jin, M.D. Xiao, Z.H. Bao, P. Wang, J.F. Wang, Angewandte Chemie International Edition 51 (2012) 6406–6410.
[5] Y.Y. Li, J.P. Liu, X.T. Huang, G.Y. Li, Crystal Growth and Design 7 (2007) 1350–1355.
[6] D.F. Zhang, L.D. Sun, J. Zhang, Z.G. Yan, C.H. Yan, Crystal Growth and Design 8 (2008) 3609–3615.
[7] J.F. Guo, J.X. Li, A.Y. Yin, K.N. Fan, W.L. Dai, Chinese Journal of Chemistry 28 (2010) 2144–2150.
[8] Y.Q. Zhu, G.T. Fei, Y. Zhang, X.M. Chen, H.B. Tang, L.D. Zhang, Journal of Physical Chemistry C 115 (2011) 13597–13602.
[9] P. Rai, H.M. Song, Y.S. Kim, M.K. Song, P.R. Oh, J.M. Yoon, Y.T. Yu, Materials Letters 68 (2012) 90–93.
[10] K.S. Kim, H. Jeong, M.S. Jeong, G.Y. Jung, Advanced Functional Materials 20 (2010) 3055–3063.
[11] A.P. Alivisatos, Science 289 (2000) 736–737.
[12] R.Q. Song, H. Colfen, Advanced Materials 22 (2010) 1301–1330.
[13] W.J. Ren, Z.H. Ai, F.L. Jia, L.Z. Zhang, X.X. Fan, Z.G. Zou, Applied Catalysis B 69 (2007) 138–144.
[14] Y. Hu, Y. Liu, H.S. Qian, Z.Q. Li, J.F. Chen, Langmuir 26 (2010) 18570–18575.
[15] M.J. Zhou, Y. Hu, Y. Liu, W.L. Yang, H.S. Qian, CrystEngComm 14 (2012) 7686–7693.
[16] J.B. Yin, X.P. Zhao, Chemistry of Materials 14 (2002) 4633–4640.
[17] P.S. Winkel, W.W. Lukens, D.Y. Zhao, P.D. Yang, B.F. Chmelka, G.D. Stucky, Journal of the American Chemical Society 121 (1999) 254–255.
[18] X.F. Zhou, Z.L. Hu, Y.Q. Fan, S. Chen, W.P. Ding, N.P. Xu, Journal of Physical Chemistry C 112 (2008) 11722–11728.
[19] M. Kruk, M. Jaroniec, Chemistry of Materials 13 (2001) 3169–3183.
[20] Y. Liu, L. Yu, Y. Hu, C.F. Guo, F.M. Zhang, X.W. Lou, Nanoscale 4 (2012) 183–187.
[21] Y. Guo, H.S. Wang, C.L. He, L.J. Qiu, X.B. Cao, Langmuir 25 (2009) 4678–4684.
[22] H.M. Xiong, Y. Xu, Q.G. Ren, Y.Y. Xia, Journal of the American Chemical Society 130 (2008) 7522–7523.
[23] X. Zhou, Y.Z. Li, T. Peng, W. Xie, X.J. Zhao, Materials Letters 63 (2009) 1747–1749.
[24] X.S. Tang, E.S.G. Choo, L. Li, J. Ding, J.M. Xue, Langmuir 25 (2009) 5271–5275.
[25] F.H. Wang, H.P. Chang, C.C. Tseng, C.C. Huang, Surface and Coatings Technology 205 (2011) 5269–5277.
[26] G. Wu, X.Y. Tana, G.Y. Li, C.W. Hu, Journal of Alloys and Compounds 504 (2010) 371–376.
[27] S. Akbar, S.K. Hasanain, M. Abbas, S. Ozcan, B. Ali, S.I. Shah, Solid State Communications 151 (2011) 17–20.
[28] S. Cho, J.W. Jang, J.S. Lee, K.H. Lee, CrystEngComm 12 (2010) 3929–3935.
[29] X.B. Liu, H.J. Du, X.W. Sun, B. Liu, D.W. Zhao, H.D. Sun, CrystEngComm 14 (2012) 2886–2890.
[30] J.L. Zhai, L.L. Wang, D.J. Wang, Y.H. Lin, D.Q. He, T.F. Xie, Sensors and Actuators B 161 (2012) 292–297.
[31] J. Zhang, L.D. Sun, J.L. Yin, H.L. Su, C.S. Liao, C.H. Yan, Chemistry of Materials 14 (2002) 4172–4177.
[32] T. Ghoshal, S. Kar, S. Chaudhuri, Crystal Growth and Design 7 (2007) 136–141.
[33] X.M. Sun, Y.D. Li, Angewandte Chemie International Edition 43 (2004) 597–601.
[34] Q. Wang, H. Li, L.Q. Chen, X.J. Huang, Solid State Ionics 152 (2002) 43–50.
[35] L.C. Jia, W.P. Cai, H.Q. Wang, H.B. Zeng, Crystal Growth and Design 8 (2008) 4367–4371.
[36] Y.H. Tseng, H.Y. Lin, M.H. Liu, Y.F. Chen, C.Y. Mou, Journal of Physical Chemistry C 113 (2009) 18053–18061.
[37] F. Waltz, G. Wißmann, J. Lippke, A.M. Schneider, H.C. Schwarz, A. Feldhoff, S. Eiden, P. Behrens, Crystal Growth and Design 12 (2012) 3066–3075.
[38] J.S. Hu, L.S. Zhong, W.G. Song, L.J. Wan, Advanced Materials 20 (2008) 2977–2982.
[39] B. Wang, H.B. Wu, L. Yu, R. Xu, T.T. Lim, X.W. Lou, Advanced Materials 24 (2012) 1111–1116.
[40] C.P. Chen, P. Gunawan, R. Xu, Journal of Materials Chemistry 21 (2011) 1218–1225.
[41] Q.H. Hu, S.Z. Qiao, F. Haghseresht, M.A. Wilson, G.Q. Liu, Industrial and Engineering Chemistry Research 45 (2006) 733–738.
[42] G. Crini, Dyes and Pigments 77 (2008) 415–426.
[43] Y.S. Ho, G.S. Mckay, Water Research 34 (2000) 735–742.
[44] W.F. Liu, J. Zhang, C.G. Zhang, Y.F. Wang, Y. Li, Chemical Engineering Journal 162 (2010) 677–684.
[45] K. Periasamy, K. Srinivasan, P.K. Murugan, Indian Journal of Environmental Health 33 (1991) 433–439.
[46] P. Yuan, M.D. Fan, D. Yang, H.P. He, D. Liu, A.H. Yuan, J.X. Zhu, T.H. Chen, Journal of Hazardous Materials 166 (2009) 821–829.
[47] B.J. Li, H.Q. Cao, J.F. Yin, Y.A. Wu, J.H. Warner, Journal of Materials Chemistry 22 (2012) 1876–1883.
[48] L. Zhou, C. Gao, W.J. Xu, ACS Applied Materials & Interfaces 2 (2010) 1483–1491.
[49] Q.F. Zhang, T.P. Chou, B. Russo, S.A. Jenekhe, G.Z. Cao, Angewandte Chemie International Edition 47 (2008) 2402–2406.
[50] K.X. Yao, H.C. Zeng, Journal of Physical Chemistry C 111 (2007) 13301–13308.
[51] W. Krengvirat, S. Sreekantan, A.M. Noor, N. Negishi, S.Y. Oh, G. Kawamura, H. Muto, A. Matsuda, International Journal of Hydrogen Energy 37 (2012) 10046–10056.
[52] J.T. Zhang, Z.G. Xiong, X.S. Zhao, Journal of Materials Chemistry 21 (2011) 3634–3640.
[53] Y. Liu, Y. Hu, M.J. Zhou, H.S. Qian, X. Hu, Applied Catalysis, B 125 (2012) 425–431.